Regulation of the filament structure and assembly of *Acanthamoeba* myosin II by phosphorylation of serines in the heavy-chain nonhelical tailpiece

Xiong Liu, Myoung-Soon Hong, Shi Shu, Shuhua Yu, and Edward D. Korn[1]

Laboratory of Cell Biology, National Heart, Lung and Blood Institute, National Institutes of Health, Bethesda, MD 20892

Contributed by Edward D. Korn, November 13, 2012 (sent for review September 17, 2012)

Acanthamoeba **myosin II (AMII) has two heavy chains ending in a 27-residue nonhelical tailpiece and two pairs of light chains. In a companion article, we show that five, and only five, serine residues can be phosphorylated both in vitro and in vivo: Ser639 in surface loop 2 of the motor domain and serines 1489, 1494, 1499, and 1504 in the nonhelical tailpiece of the heavy chains. In that paper, we show that phosphorylation of Ser639 down-regulates the actin-activated MgATPase activity of AMII and that phosphorylation of the serines in the nonhelical tailpiece has no effect on enzymatic activity. Here we show that bipolar tetrameric, hexameric, and octameric minifilaments of AMII with the nonhelical tailpiece serines either phosphorylated or mutated to glutamate have longer bare zones and more tightly clustered heads than minifilaments of unphosphorylated AMII, irrespective of the phosphorylation state of Ser639. Although antiparallel dimers of phosphorylated and unphosphorylated myosins are indistinguishable, phosphorylation inhibits dimerization and filament assembly. Therefore, the different structures of tetramers, hexamers, and octamers of phosphorylated and unphosphorylated AMII must be caused by differences in the longitudinal stagger of phosphorylated and unphosphorylated bipolar dimers and tetramers. Thus, although the actin-activated MgATPase activity of AMII is regulated by phosphorylation of Ser639 in loop 2 of the motor domain, the structure of AMII minifilaments is regulated by phosphorylation of one or more of four serines in the nonhelical tailpiece of the heavy chain.**

As summarized in the accompanying paper (1), *Acanthamoeba* myosin II (AMII) is a typical class II myosin with two heavy chains and two pairs of light chains (2, 3). The coiled-coil helical tails of the heavy chains terminate with a 27-residue nonhelical tailpiece, 1483PSSRGGSTRGASARGASVRAGSARAEE1509, which has a pattern of four contiguous repeats of XXSXR (4). Previous work had shown that phosphorylation of two or more of these serines (residues 1489, 1494, 1499, and 1504) correlates with, and was assumed to be responsible for, inactivation of AMII's actin-activated MgATPase activity (5, 6). Also, it had been concluded that only filamentous AMII has actin-activated MgATPase activity (7, 8), and it was inferred that the ATPase activity is regulated by a change in the conformation of the bipolar minifilaments (9–11). However, detailed studies by the Pollard laboratory found no significant differences in either the polymerization properties or electron microscopic images of minifilaments of phosphorylated and dephosphorylated myosins (12–16).

The earlier studies were carried out with purified endogenous myosin. To avoid possible complications in enzymatic and structural studies caused by the partial phosphorylation of purified endogenous myosin and incomplete dephosphorylation by phosphatase, we initiated studies on the enzymatic activity and structure of expressed recombinant wild-type, truncated, and mutant myosins before and after phosphorylation. As reported in the accompanying paper (1), we identified a previously unknown phosphorylation site, Ser639 in loop 2 of the motor domain, in both endogenous AMII and expressed AMII phosphorylated in vitro, in addition to the nonhelical tailpiece serine. We showed further that the actin-activated MgATPase activity of AMII is down-regulated by phosphorylation of Ser639 and not by phosphorylation of the serines in the nonhelical tailpiece. Moreover, we found that nonfilamentous AMII derivatives, heavy meromyosin and subfragment-1, also have actin-activated MgATPase activity that is down-regulated by phosphorylation of Ser639 (1).

Thus, neither phosphorylation of serines in the nonhelical tailpiece nor a phosphorylation-induced conformational change in filament structure is required for either the actin-activated ATPase activity of AMII or its inhibition by phosphorylation. However, we show in this paper that phosphorylation or mutation to glutamate of the C-terminal serines in the nonhelical tailpiece does modify substantially the structure of minifilaments of both endogenous and recombinant AMII independent of the phosphorylation status of Ser639. Although nonhelical tailpieces of other myosin IIs have been shown to be phosphorylated in vitro and in vivo (*Discussion*), the data reported in this paper demonstrate an effect of phosphorylation of a nonhelical tailpiece on the filament structure of a full-length myosin II.

Results

To address the effect of heavy-chain phosphorylation on filament structure, we used endogenous WT AMII (eWT) and recombinant WT, WT with Ser1489, 1494, 1499, and 1504 mutated to glutamic acid (4S/E), WT with Ser1489, 1494, 1499, and 1504 mutated to alanine (4S/A), WT with Ser639 mutated to aspartic acid (S639D), and WT with the nonhelical tailpiece deleted (ΔNHT). All the purified proteins were electrophoretically homogenous (Fig. 1).

Effect of Mg^{2+} on Microfilament Assembly. In 10 mM imidazole (pH 7.0), 2.5 mM KCl, 1 mM ATP, and no Mg^{2+}, WT, S639D and 4S/A formed predominantly antiparallel bipolar tetramers and hexamers (~80%) with no minifilaments larger than hexamers (Fig. 2 and Table 1). However, phosphorylated WT and S639D (pWT and pS639D, respectively) and the phosphomimetic mutant 4S/E were predominantly monomers (~90%) with a few tetramers but no hexamers or octamers (Fig. 2). Addition of $MgCl_2$ substantially increased the percentages of tetramers (Figs. 3 and 4 and Table 1) and octamers (Figs. 5 and 6 and Table 1). WT, S639D, and 4S/A

Significance

Class II myosins are the only members of this superfamily of actin-associated molecular motors that form antiparallel bipolar filaments, which are essential for the biological functions of these myosins. Here we show that the assembly of *Acanthamoeba* myosin II monomers into minifilaments is modified by phosphorylation of one or more of four serine residues in the 27-residue nonhelical tailpiece at the end of each of the two heavy chains that form the coiled-coil helix characteristic of class II myosins. This regulatory mechanism might be applicable to other class II myosins that have a nonhelical tailpiece.

Author contributions: X.L. and E.D.K. designed research; X.L., M.-S.H., S.S., and S.Y. performed research; X.L., M.-S.H., S.S., and E.D.K. analyzed data; and X.L. and E.D.K. wrote the paper.

The authors declare no conflict of interest.

[1]To whom correspondence should be addressed. E-mail: korne@nhlbi.nih.gov.

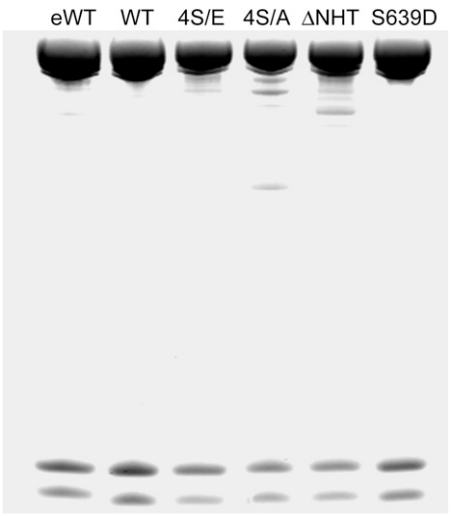

Fig. 1. SDS/PAGE of endogenous *Acanthamoeba* myosin II and recombinant myosins. Samples were analyzed on a 1.0-mm 10% NuPAGE gel (Life Technologies). WT and purified recombinant myosins were expressed in Sf-9 cells. The gel was stained with Coomassie blue.

formed tetramers and octamers at a lower concentration of $MgCl_2$ than their phosphorylated or phosphomimetic equivalents pWT, pS639D, and 4S/E (0.5 and 1 mM vs. 1 and 2 mM for tetramers and octamers, respectively; Table 1). The ΔNHT construct behaved similarly to WT (Fig. 5).

Phosphorylation Affects the Structure of Tetramers and Octamers. As summarized in Table 2, the dimensions of monomers and dimers in 10 mM imidazole (pH 7.0), 2.5 mM KCl, 1 mM ATP, and 0.5–2 mM $MgCl_2$ were very similar for all six AMII constructs. The tail length of all monomers varied between 88 and 91 nm, and all constructs formed antiparallel dimers with a bare zone of 157–162 nm and an overlap of 14–21 nm, as previously reported by Sinard et al. (14) for WT polymerized in 25 mM KCl and no $MgCl_2$. However, there were significant differences in the structures of tetramers and octamers of unphosphorylated and phosphorylated and phosphomimetic myosin.

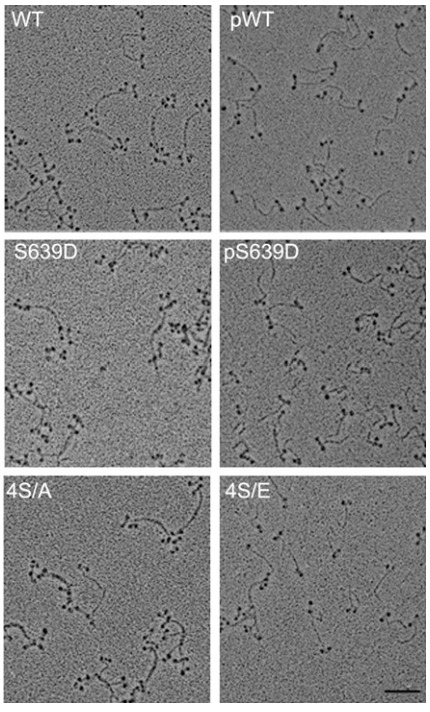

Fig. 2. Electron microscopic images of rotary-shadowed AMII constructs in 10 mM imidazole (pH 7.0), 2.5 mM KCl, 1 mM ATP, and no $MgCl_2$. WT, S639D, and 4S/A are mostly tetramers and hexamers (~80%; Table 1), and their phosphorylated or phosphomimetic counterparts, pWT, pS639D, and 4S/E, are mostly monomers (~90%; Table 1). (Scale bar, 100 nm.)

Table 1. Effect of ionic conditions on the assembly of WT and pWT AMII

Condition	Monomer (%)	Dimer (%)	Tetramer (%)	Hexamer (%)	Octamer (%)
0.25 mM KCl					
WT	11	10	41	39	0
pWT	90	9	1	0	0
0.25 mM KCl, 0.5 mM $MgCl_2$					
WT	2	3	26	64	5
pWT	84	10	6	0	0
0.25 mM KCl, 1.0 mM $MgCl_2$					
WT	0	0	3	13	84
pWT	3	1	79	5	12
0.25 mM KCl, 2.0 mM $MgCl_2$					
WT	0	0	0	0	23*
pWT	5	0	2	9	84
25 mM KCl					
WT	0	0	20	30	50
pWT	0	0	80	15	5

All samples contained 10 mM imidazole (pH 7.0) and 1 mM ATP except for the 25 mM KCl sample. Percentages are based on more than 200 structures in 8–50 fields.
*The remaining filaments were larger than octamers.

Tetramers of WT, ΔNHT, S639D, and 4S/A had bare zones of 141–143 nm and a stagger of 15–19 nm between dimers (Figs. 3 and 4 and Table 2), as previously reported by Sinard et al. (14) for WT polymerized in KCl and no $MgCl_2$. In contrast, tetramers of pWT, pS639D, and 4S/E had longer bare zones of 153–158 nm, each 12–15 nm longer than in its unphosphorylated or phosphomimetic counterpart and similar to the lengths of the bare zones of the dimers (Figs. 3 and 4 and Table 2). Also, the four heads at each end of bipolar tetramers of pWT, pS639D, and 4S/E were clustered more tightly than the heads of WT, S639D, 4S/A, and ΔNHT, with areas of 650–900 nm^2 compared with areas of 1,100–1,300 nm^2 (Figs. 3 and 4 and Table 2). Similarly, the bare zones of phosphorylated octamers were longer (125–128 nm vs. 100–102 nm), and the areas of their heads were smaller (1,300–1,600 nm^2 vs. 1,700–2,200 nm^2) than in the corresponding unphosphorylated octamers (Figs. 5 and 6 and Table 2).

At higher concentrations of $MgCl_2$, octameric minifilaments aggregate laterally forming thick filaments (12, 13). As with tetrameric and octameric minifilaments, the thick filaments of unphosphorylated WT differed from thick filaments of pWT and 4S/E (Fig. 7). Thick filaments of pWT and 4S/E had tight clusters of multiple heads and a distinct bare zone, whereas the heads in WT thick filaments were fairly widely dispersed obscuring the bare zone.

In the previous studies that reported no differences in electron micrographs of WT and pWT filaments (12, 13), assembly was in 20–25 mM KCl with neither $MgCl_2$ nor ATP, whereas the filaments in Figs. 3–6 were assembled in 10 mM imidazole (pH 7.0), 2.5 mM KCl, 1–2 mM $MgCl_2$, and 1 mM ATP. Therefore we compared electron micrographs of rotary-shadowed WT and pWT minifilaments polymerized in 25 mM KCl and no $MgCl_2$ or ATP (Fig. 8). We found that the heads were more tightly clustered and the bare zones were longer in tetramers and hexamers of pWT than of WT. In 25 mM KCl and no $MgCl_2$, the bare zones of tetramers were 141 and 154 nm, and the areas of the four heads at each end of the

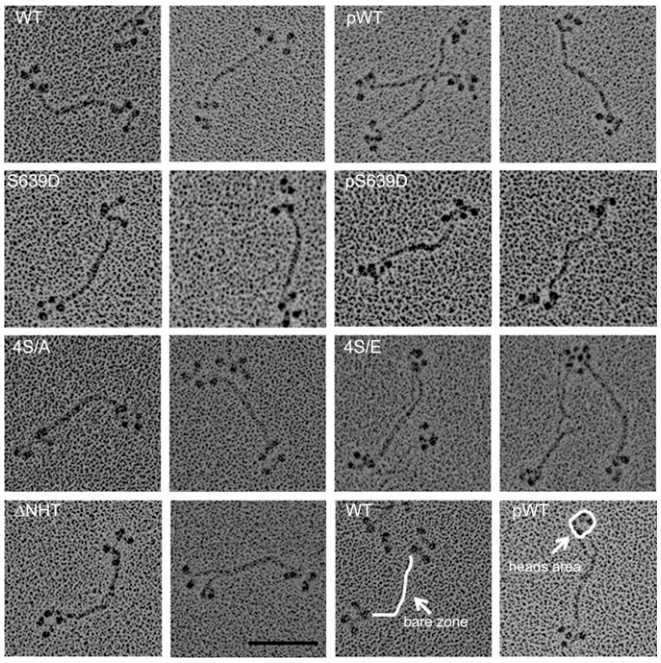

Fig. 3. Electron microscopic images of rotary-shadowed tetramers of AMII constructs. To maximize tetramer formation, WT, S639D, and 4S/A were polymerized in 10 mM imidazole (pH 7.0), 2.5 mM KCl, 1 mM ATP, and 0.5 mM $MgCl_2$, and pWT, pS639D, and 4S/E were polymerized in 10 mM imidazole (pH 7.0), 2.5 mM KCl, 1 mM ATP, and 1.0 mM $MgCl_2$. Two images are shown for each construct; the construct is identified in the left panel of the pair. The white lines in the WT and pWT images at the lower right illustrate how the lengths of the bare zones and the areas of the heads at each end were measured. The bare zones are longer and the heads are more tightly clustered in pWT, pS639D, and 4S/E than in WT, S639D, and 4S/A (Table 2). (Scale bar, 100 nm.)

tetramers were 942 and 605 nm^2 for WT and pWT, respectively (Table 2). For hexamers, the bare zones were 120 and 145 nm, and the head areas were 1,394 and 1,032 nm^2 for WT and pWT, respectively (Table 2). Note that the heads of tetramers of both WT and pWT were clustered more tightly in 25 mM KCl than in 2.5 mM KCl or 1–2 mM $MgCl_2$ (Table 2). There were too few monomers, dimers, and octamers in pWT to obtain statistically significant numbers, but individual octamers of WT and pWT showed differences similar to those seen in tetramers and hexamers (Fig. 8).

Phosphorylation and Dephosphorylation of Filaments. The data on phosphorylated myosin minifilaments discussed above were obtained with samples phosphorylated as monomers and then dialyzed and diluted in appropriate buffers to form filaments. To determine if the structure of myosin filaments was affected by phosphorylation and dephosphorylation at the filament level, we phosphorylated WT myosin after polymerization to octamers in 1 mM $MgCl_2$ as shown in Figs. 5 and 6. After phosphorylation, the octamers disappeared and were replaced by monomers, antiparallel dimers (not shown), and clumped tetramers and hexamers (Fig. 9, pWT). When pWT was incubated with phosphatase, staggered tetramers, hexamers, and octamers reappeared (Fig. 9, dpWT). We conclude that phosphorylation and dephosphorylation of filaments alter filament structure directly or that the structural changes occur as a result of a dynamic equilibrium between filamentous and monomeric phosphorylated and dephosphorylated myosins. In either case, it seems likely that phosphorylation and dephosphorylation of the C-terminal tailpiece could affect myosin filament structure in vivo.

Minifilaments of Endogenous AMII Have Varied Structures. We previously reported (6) that the serines in the nonhelical tailpiece of endogenous AMII are partially phosphorylated and that purified endogenous AMII has very low actin-activated MgATPase activity. We now show that purified endogenous AMII monomers assembled in 1 mM imidazole (pH 7.0), 1 mM $MgCl_2$, and 1 mM ATP form a mixture of tetramers, hexamers, and octamers (Fig. 10). Some filaments had staggered heads and bare zones similar to filaments of expressed WT AMII, whereas others had clumped heads and longer bare zones similar to filaments of pWT AMII. This heterogeneity of filament structure is not surprising given the heterogeneity of phosphorylation of the nonhelical tailpiece of endogenous AMII reported in the accompanying paper (1): 44% of the heavy chains of eWT had no phosphorylated serines in their nonhelical tailpiece, and the average level of phosphorylation of nonhelical tailpiece serines was only 0.9 P per heavy chain. Assuming random phosphorylation in vivo, 99% of the purified monomers and all filaments assembled in vitro would have been phosphorylated on at least one nonhelical tail serine (1).

Discussion

The assembly of full-length *Acanthamoeba* myosin II was studied extensively by Pollard and colleagues (12–16). They found that minifilaments (octamers) were formed in three steps when polymerized in ≤100 mM KCl and no ATP or $MgCl_2$: Two monomers formed an antiparallel dimer with an ∼15-nm overlap of their tails and a bare zone of ∼160 nm; two dimers formed an antiparallel tetramer with a bare zone of ∼140 nm and an ∼15-nm stagger between the dimers; and two tetramers associated to form an antiparallel octamer with a bare zone of ∼117 nm and a stagger between tetramers of ∼30 nm. Our results for the polymerization

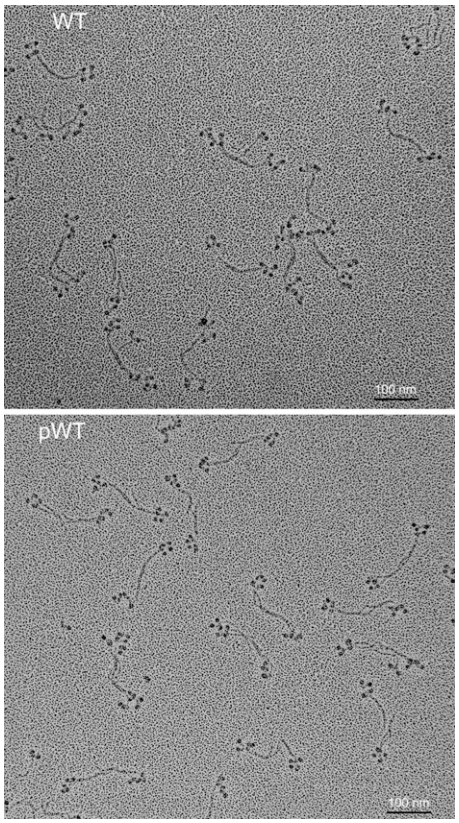

Fig. 4. Field electron microscopic image of rotary-shadowed AMII. (*Upper*) Unphosphorylated WT in 10 mM imidazole (pH 7.0), 2.5 mM KCl, 1 mM ATP, and 0.5 mM $MgCl_2$; staggered, antiparallel bipolar hexamers and tetramers are present. (*Lower*) pWT in 10 mM imidazole (pH 7.0), 2.5 mM KCl, 1 mM ATP, and 1 mM $MgCl_2$; mostly clumped antiparallel tetramers with little stagger are seen. (Scale bars, 100 nm.)

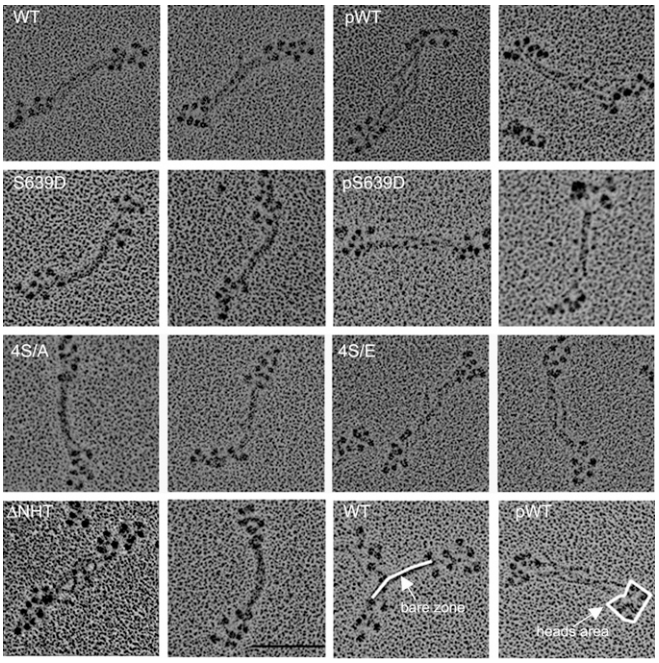

Fig. 5. Electron microscopic images of rotary-shadowed octamers of AMII constructs. To maximize octamer formation, WT, S639D, 4S/A, and ΔNHT were polymerized in 10 mM imidazole (pH 7.0), 2.5 mM KCl, 1 mM ATP, and 1 mM $MgCl_2$, and pWT, pS639D, and 4S/E were polymerized in 10 mM imidazole (pH 7.0), 2.5 M KCl, 1 mM ATP, and 2 mM $MgCl_2$. The bare zones are longer and the heads more tightly clustered in pWT, pS639D, and 4S/E than in WT, S639D, and 4S/A (Table 2). Panels are labeled as in Fig. 3. (Scale bar, 100 nm.)

of unphosphorylated WT in both 25 mM KCl and in 2.5 mM KCl, 1 mM ATP, and 1–2 mM $MgCl_2$ are similar.

In the earlier studies, no significant differences were observed between the polymerization of purified endogenous (partially phosphorylated) myosin and endogenous myosin dephosphorylated in vitro. However, we found that both WT and pWT form hexamers and that a higher concentration of $MgCl_2$ is required for pWT to form octamers (Table 1). Most interestingly, we found that the bare zones of tetramers, hexamers, and octamers of phosphorylated AMII are longer and their heads more tightly clustered than those of unphosphorylated AMII (Table 2). 4S/E filaments mimic pWT filaments, and 4S/A filaments mimic unphosphorylated WT filaments. Similar differences were found between pS639D and S639D. Thus, these differences in minifilament structure are caused entirely by the phosphorylation of serines in the nonhelical tailpiece and are entirely independent of phosphorylation of S639, which was shown in the accompanying paper (1) to down-regulate actin-activated ATPase activity, which is not affected by phosphorylation of the nonhelical tailpiece serines.

The longer bare zones of tetramers and octamers (but not dimers) of phosphorylated AMII relative to unphosphorylated AMII suggests that clustering of heads results from a change of alignments of dimers and tetramers in the formation of minifilaments. Dimers and tetramers of phosphorylated myosins align side-by-side, forming tetramers and octamers with a significantly smaller, and perhaps less uniform, stagger than seen in the alignment of dimers and tetramers of unphosphorylated myosin (Fig. 11).

As mentioned above, we found that hexamers accounted for 39% of unphosphorylated recombinant WT minifilaments assembled in 2.5 mM KCl and 1 mM ATP (Fig. 2 and Table 1) and that both WT and pWT formed hexamers as well as tetramers and octamers in 25 mM KCl without ATP (Fig. 8 and Table 1) and in 2.5 mM KCl, 1 mM $MgCl_2$, and 1 mM ATP (Figs. 6 and 10 and Table 1). Like tetramers, the heads of pWT hexamers were clumped together with little stagger (Figs. 3–6 and 8). To account for the presence of hexamers and for the different structures of tetramers and octamers of phosphorylated and nonphosphorylated myosins, we suggest the existence of an alternative assembly pathway (Fig. 11) in which octamers would be formed by sequential addition of dimers to tetramers and hexamers.

The differences between our results and previous results may be caused by the presence of 0 and 8 mol P/mol of myosin in our unphosphorylated and phosphorylated myosins, respectively, whereas the dephosphorylated and phosphorylated myosins (i.e., isolated endogenous myosin) in previous studies had 0.8–1.2 and 3–5 mol P/mol of myosin, respectively, which would have included phosphorylated Ser639 (1). The smaller differences in the levels of phosphorylation of dephosphorylated and phosphorylated myosin in the previous studies and the probability that both myosins would assemble into significantly heterogeneous filaments, as we show in this paper for isolated endogenous myosin, would have made it more difficult to detect structural differences between phosphorylated and dephosphorylated myosin in the earlier studies.

Heavy-chain phosphorylation also occurs in several other myosin IIs, i.e., *Dictyostelium*, *Physarum*, and vertebrate myosins II A, B, and C (17), but at different positions in the heavy chain and with different regulatory consequences. Phosphorylation of three threonine residues in the middle of the helical rod of *Dictyostelium* myosin II promotes bending of the rod and disassociation of the filaments (18), and disassembly makes the actin-activated ATPase activity independent of light-chain phosphorylation (19). Disassembly of *Dictyostelium* myosin II filaments by tail phosphorylation is similar to the decrease in the size of AMII mini-

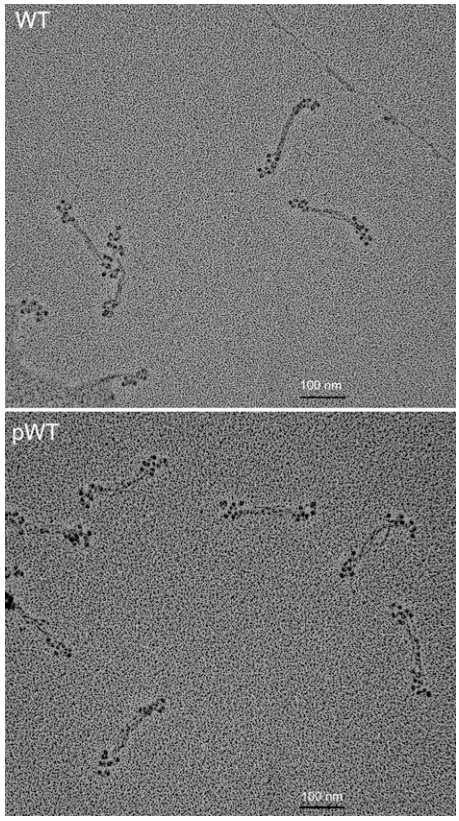

Fig. 6. Field electron microscopic image of rotary-shadowed AMII. (*Upper*) WT in 10 mM imidazole (pH 7.0), 2.5 mM KCl, 1 mM $MgCl_2$, and 1 mM ATP shows staggered bipolar octamers. (*Lower*) pWT in 10 mM imidazole (pH 7), 2.5 mM KCl, 2 mM $MgCl_2$, and 1 mM ATP shows antiparallel bipolar octamers with clustered heads. (Scale bars, 100 nm.)

Table 2. Dimensions of monomers, dimers, tetramers, octamers, and hexamers of *Acanthamoeba* myosin II constructs

			Tetramer		Octamer		Hexamer*	
Myosin	Monomer Tail (nm)	Dimer bare zone (nm)	Bare zone (nm)	Head area (nm^2)	Bare zone (nm)	Head area (nm^2)	Bare zone (nm)	Head area (nm^2)
WT	87.8 ± 2.1 (30)	162.4 ± 3.3 (25)	141.2 ± 6.1 (120)	1,247.7 ± 182.4 (110)	101.7 ± 5.9 (73)	1,976.4 ± 240 (56)		
pWT	89.2 ± 2.7 (31)	161.6 ± 2.4 (22)	158.3 ± 4.4 (106)	881.9 ± 166.5 (135)	128.2 ± 7.2 (112)	1,582.9 ± 252 (106)		
S639D	89.3 ± 1.5 (23)	158.5 ± 3.7 (20)	140.8 ± 4.2 (50)	1,081.0 ± 207.8 (102)	99.7 ± 2.9 (76)	2,210.6 ± 298 (112)		
pS639D	89.3 ± 2.4 (30)	156.8 ± 4.7 (28)	153.1 ± 5.1 (110)	718.3 ± 113.6 (110)	125.1 ± 7.4 (118)	1,465.0 ± 237.4 (94)		
4S/A	88.5 ± 2.8 (30)	158.9 ± 2.4 (16)	139.5 ± 3.8 (41)	1,162.5 ± 158.9 (108)	98.6 ± 4.0 (91)	1,863.1 ± 229.9 (114)		
4S/E	91.0 ± 2.5 (26)	162.3 ± 2.7 (18)	154.7 ± 3.7 (110)	655.0 ± 125.1 (152)	127.2 ± 7.8 (150)	1,275.2 ± 251.4 (100)		
ΔNHT	90.3 ± 2.3 (32)	161.1 ± 3.7 (39)	143.2 ± 3.7 (60)	1,213.9 ± 186.3 (102)	99.6 ± 5.1 (86)	1,748.5 ± 191.3 (94)		
WT*	ND	ND	140.6 ± 2.8 (30)	942.4 ± 207.3 (90)	ND	ND	119.8 ± 3.1 (64)	1,393.5 ± 143.1 (100)
pWT*	ND	ND	154.3 ± 3.6 (70)	605.4 ± 108.3 (100)	ND	ND	144.6 ± 4.2 (32)	1,031.9 ± 231.5 (68)

All samples were polymerized in 10 mM imidazole (pH 7.0), 2.5 mM KCl, 1 mM ATP, and 0.5, 1, or 2 mM $MgCl_2$ as stated in the legends of Figs. 3 and 4, except as indicated in the footnote. Data are reported as mean ± SD with the number of samples measured in parentheses. The sample numbers are smaller for monomers and dimers, because, under the conditions used, tetramers and octamers are strongly favored.
ND, not determined.
*Polymerized in 10 mM imidazole, pH 7.0, and 25 mM KCl but not in either ATP or $MgCl_2$; there were too few monomers, dimers, and octamers of pWT to obtain significant data.

filaments caused by phosphorylation of the nonhelical tailpiece serines that we observed (Table 1). The phosphorylated amino acids in *Physarum* myosin II have not been identified, but, in contrast to *Acanthamoeba* and *Dictyostelium* myosin IIs, heavy-chain phosphorylation of *Physarum* myosin II enhances its actin-activated MgATPase activity and facilitates its assembly (20).

Mammalian nonmuscle myosin IIs, NMIIA, NMIIB, and NMIIC, also are phosphorylated on their C-terminal nonhelical tailpieces (21). Most of the reports on the role of the nonhelical tailpieces of vertebrate myosin IIs are based on in vitro studies of tail fragments of the mammalian nonmuscle myosin IIs NMIIA, NMIIB, and, to a lesser extent, NMIIC (22–27). Phosphorylation by protein kinase C or casein kinase II of one or more serines in the nonhelical tailpieces of NMIIA and NMIIB was reported to inhibit assembly of NMIIB tail fragments but not of NMIIA tail fragments (23, 24), as assayed by sedimentation, but in a later study was reported to inhibit the assembly of tail fragments of NMIIA (25). Deletion of the nonhelical tailpiece was reported to promote the assembly of the 640-residue tail fragments of NMIIA and NMIIB but to weaken the assembly of the 604-residue tail fragment of NMIIC (26), as had been reported earlier for deletion of the nonhelical tailpiece from the 397-residue tail fragment of chicken brush border myosin II (27). However, the assembly properties of tail fragments, which form parallel arrays of filaments in paracrystals (26), may not be a useful model for the polymerization of full-length myosin IIs, which form bipolar, antiparallel minifila-

Fig. 7. Electron microscopic images of negatively stained WT, pWT, and 4S/E as a function of $MgCl_2$ concentration. All constructs were polymerized in 10 mM imidazole (pH 7.0), 2.5 mM KCl, 1 mM ATP, and varied $MgCl_2$ concentrations as indicated in the figure. The minifilaments of all constructs aggregated laterally in 6 and 10 mM $MgCl_2$ to form thick filaments, but the heads of pWT and 4S/E are more clustered, and the bare zones are more distinct for WT than for pWT and 4S/E. (Scale bar, 100 nm.)

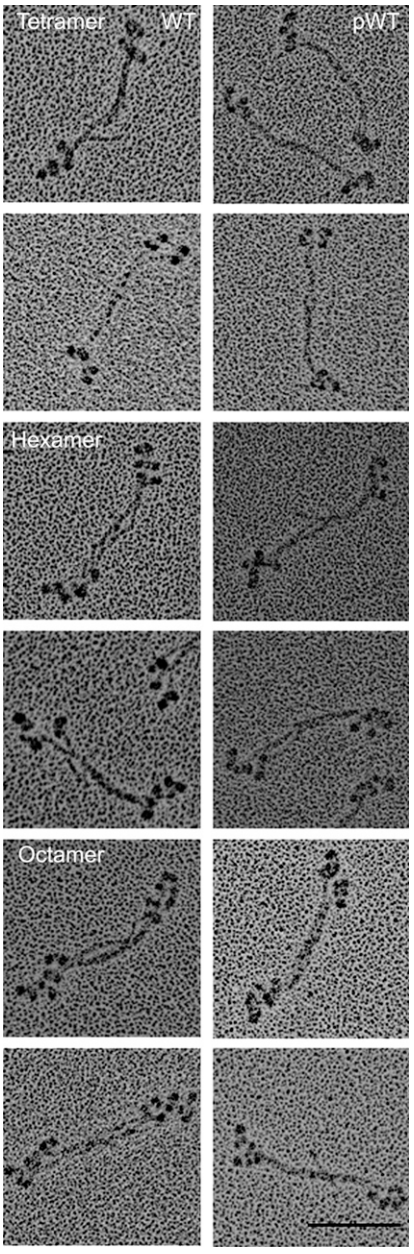

Fig. 8. Minifilaments of WT and pWT in 10 mM imidazole (pH 7.0) and 25 mM KCl without $MgCl_2$ or ATP. WT forms tetramers, hexamers, and octamers. pWT forms mostly tetramers, some hexamers, and very few octamers. The heads are more clustered and the bare zones are longer in pWT minifilaments than in the corresponding WT minifilaments. (Scale bar, 100 nm.)

ments. The effects, if any, of phosphorylation of the nonhelical tailpiece on the filament structure of full-length myosins were not investigated in these studies. In our study deletion of the nonhelical tail piece (ΔNHT) did not change the dimensions and shapes of monomers, dimers, tetramers, and octamers of *Acanthamoeba* myosin II (Figs. 3 and 5 and Table 2).

At least some of the serines in the nonhelical tailpieces of mammalian nonmuscle myosin IIs that are phosphorylated in vitro are phosphorylated in vivo in bovine brain (22), in cultured rodent cells (28), in HeLa cells (29), and in human breast cancer cells (30). Breast cancer cells expressing the NMIIA phosphomimetic mutants S1943E and S1943D (Ser1943 is a nonhelical tailpiece site that is phosphorylated in vivo) had increased migration and enhanced lamellipodia formation, whereas migration and lamellipodia were reduced in cells expressing the S1943A mutant (30). Moreover, S1943A and ΔNHT mutants of NMIIA overassemble with altered intracellular localization when expressed in HeLa cells (29), and phosphomimics at phosphoserine sites regulated the assembly and location of NMII rods expressed in mouse embryonic fibroblasts (26), although these mutations did not affect the paracrystal structure of the rods in vitro. Quite recently, it was observed that NMIIA is diffuse and mobile in mesenchymal stem cells crawling on a soft matrix but strongly assembled in oriented stress fibers in cells crawling on a stiff matrix (31). The shift from diffuse to assembled NMIIA correlated with, and apparently was caused by, a decrease in phosphorylation of S1943.

In summary, we have shown in the accompanying paper (1) that the heavy chain of both endogenous AMII purified from amoeba and recombinant AMII incubated with kinase in vitro are phos-

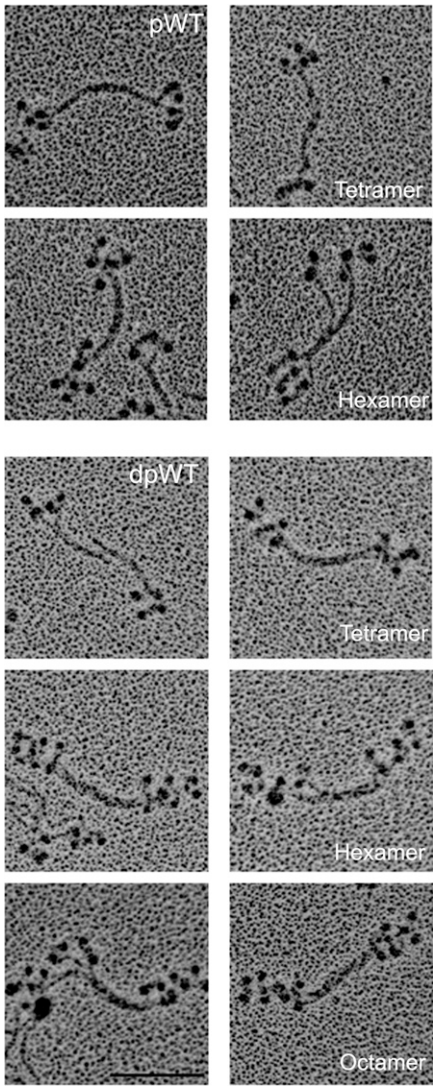

Fig. 9. Change in structure of minifilaments of recombinant AMII upon phosphorylation and dephosphorylation. Filaments of unphosphorylated WT in 10 mM imidazole (pH 7.0), 2.5 mM KCl, 1 mM ATP, and 1 mM $MgCl_2$ were phosphorylated by AMII heavy-chain kinase (pWT) and then were dephosphorylated by phosphatase (dpWT). (*Upper*) pWT: Phosphorylation converted staggered octamers (as shown in WT, Figs. 5 and 6) into a mixture of monomers (~8%) and dimers (~9%) (not shown) and, clumped tetramers (~39%), and clumped hexamers (~44%). (*Lower*) dpWT: Dephosphorylation reconverted pWT into a mixture of staggered tetramers (~14%), hexamers (~13%), and octamers (~73%), as shown in paired images for each structure. (Scale bar, 100 nm.)

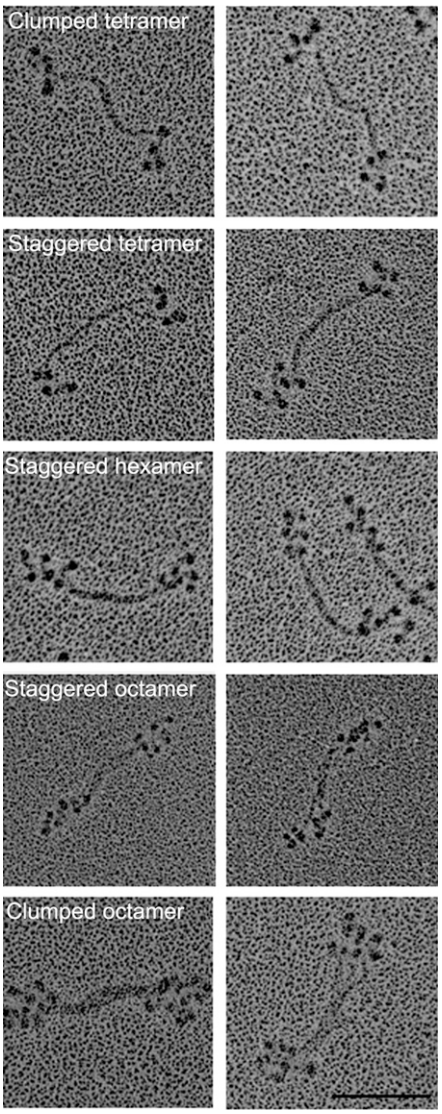

Fig. 10. Isolated eWT AMII forms a heterogeneous mixture of minifilaments. Purified eWT monomers assembled in 10 mM imidazole (pH 7.0), 2.5 mM KCl, 1 mM ATP, and 1 mM $MgCl_2$ form a mixture of clumped and staggered tetramers, hexamers, and octamers. Two images are shown for each structure; structures are identified in the left panels. (Scale bar, 100 nm.)

phorylated on Ser639 in the motor domain and one or more of serines 1489, 1494, 1499, and 1504 in the nonhelical tailpiece and that phosphorylation of Ser639 specifically down-regulates its actin-activated ATPase activity. In this paper we show that tetramers, hexamers, and octamers of recombinant AMII phosphorylated on the nonhelical tailpiece serines have shorter bare zones and more tightly clustered heads than the corresponding minifilaments of nonphosphorylated AMII. Although phosphorylated monomers and dimers are indistinguishable by electron microscopy, phosphorylation of the nonhelical tailpiece serines inhibits both dimerization of monomers and assembly of dimers into minifilaments. Purified endogenous myosin monomers assemble in vitro into a mixture of filaments resembling homopolymers of phosphorylated and unphosphorylated myosins, and dephosphorylation and rephosphorylation of assembled filaments in vitro transforms them into structures similar to the structures of unphosphorylated and phosphorylated filaments.

Although we have not studied the biological consequences of phosphorylation of the nonhelical tailpiece of AMII in vivo, phosphorylation might cause partial or complete filament disassembly, modify filament localization, regulate the interaction of filaments with myosin-binding proteins, and/or fine-tune actin-activated MgATPase activity that is regulated principally by phosphorylation of Ser639 in the motor domain. Relevant to the first two possibilities, the Pollard laboratory (32, 33) observed by light microscopy of labeled AMII expressed in *Acanthamoeba* that thick filaments (i.e., assembled minifilaments) formed at the leading edge of motile cells and accumulated and disassembled at the rear. However, thick filaments of AMII with three of the nonhelical tailpiece serines mutated to glutamate preferentially clustered around vesicles. Minifilaments (presumably octamers) were dispersed more uniformly throughout the cytoplasm. These observations are consistent with the expectation from our results that phosphorylation of the nonhelical tailpiece would induce dissociation of AMII filaments, given the ionic composition of *Acanthamoeba* cytoplasm (34, 35), and are also consistent with the effects of phosphorylation of Ser1943 in the nonhelical tailpiece of mammalian NMIIA discussed above.

Finally, we do not know if the same enzyme in the partially purified heavy-chain kinase used in this research phosphorylates

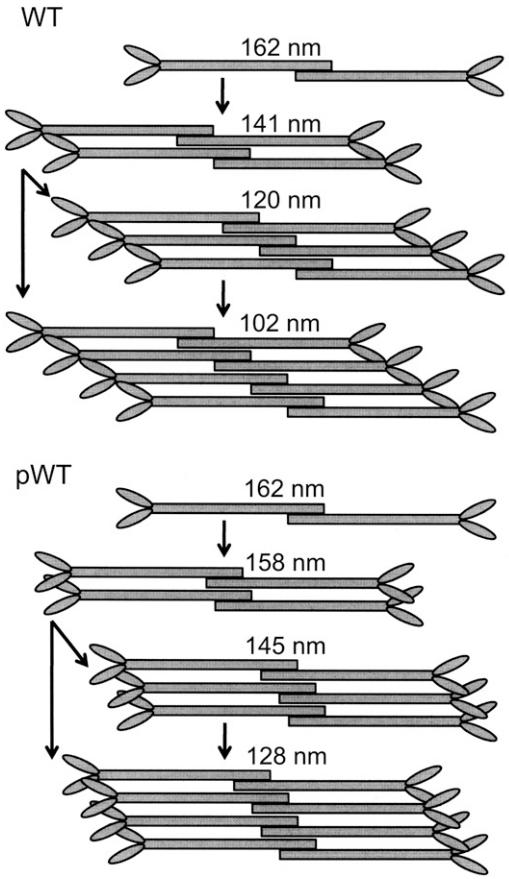

Fig. 11. Alternative assembly pathways for the formation of minifilaments of unphosphorylated and phosphorylated AMII. Dimers of WT and pWT are indistinguishable, but assembly of pWT (*Lower*) forms tetramers, hexamers, and octamers with a smaller stagger than seen in WT minifilaments (*Upper*). As a result, the bare zones are longer and the heads are more tightly clustered in pWT minifilaments than in WT minifilaments. Octamers might be formed by the interaction of two tetramers, by the sequential addition of dimers to tetramers and hexamers, or by both processes. The length of the bare zones of dimers, tetramers, and octamers are the median values in Table 2 for assembly in $MgCl_2$ and ATP. The lengths of the bare zones of hexamers are from filament assembly in 25 mM KCl (Table 2); too few well-shaped hexamers were formed in filament assembly in $MgCl_2$ and ATP to calculate a median value.

both Ser639 and the serines in the nonhelical tailpiece. If only one kinase is responsible for all the phosphorylations, down-regulation of actin-activated MgATPase activity and changes in filament structure most probably would occur simultaneously and be complementary. If different kinases are involved, then the two enzymes could be activated independently, and the enzymatic activity and filament structure of AMII could be independently regulated.

Materials and Methods

Protein Preparation. Mutation of AMII heavy chain, expression and purification of WT and mutant AMII, purification of endogenous AMII from *Acanthamoeba*, purification of AMII heavy-chain kinase, and phosphorylation of monomeric myosin and SDS/PAGE analysis of myosin constructs are described in the accompanying paper (1).

Phosphorylation of Filamentous WT and Dephosphorylation of Filamentous pWT. Recombinant myosin (0.6 mg/mL) was dialyzed against 10 mM imidazole (pH 7.0) and 25 mM KCl overnight. It then was diluted 10-fold in a solution containing 1 mM $MgCl_2$, 1 mM ATP, 2.5 mM KCl, and 10 mM imidazole (pH 7.0). A 100-μL aliquot was incubated with 5 μL of 10-fold–diluted kinase preparation at 30 °C in a shaker for 1 h. Then 0.6 mg/mL of the resultant pWT was dissolved in a buffer of 1 mM $MgCl_2$, 1 mM ATP, 2.5 mM KCl, and 10 mM imidazole (pH 7.0). An 40-μL aliquot was mixed with 5 μL of 10× concentrated phosphatase buffer (New England BioLabs) and 5 μL of 10× concentrated $MnCl_2$ solution (New England BioLabs) and was incubated with 1 μL of lambda protein phosphatase (New England BioLabs) for 10 min at room temperature.

Electron Microscopy. For electron microscopy, myosins were dialyzed against 10 mM imidazole (pH 7.0) and 25 mM KCl overnight and then were mixed with ATP and $MgCl_2$ to a final concentration of 120 nM myosin, 10 mM imidazole (pH 7.0), 1 mM ATP, 2.5 mM KCl, and $MgCl_2$ as indicated. To obtain negatively stained samples, Formvar/carbon-coated 400-mesh copper grids were glow-discharged for 30 s in an EMScope TB500 sputter coater (EMScope Laboratories), and 5 μL of protein solution (0.1 mg/mL) was applied. After a few seconds, the excess liquid was absorbed with filter paper. The grid was stained with a drop of 1% aqueous uranyl acetate for 30 s, the excess stain was removed with filter paper, and the sample was observed in a JEM-1200EX II transmission electron microscope (JEOL). Micrographs were recorded at a nominal magnification of 50,000× at 80 kV.

To prepare rotary-shadowed samples, one volume of protein (0.1–1.0 mg/mL) was mixed with two volumes of glycerol, sprayed onto a mica sheet and then placed in the high-vacuum chamber of a rotary shadowing machine (RFD-9010, RMC; Boeckeler Instruments, Inc.). The sample was shadowed with platinum-carbon at an angle of 9° for 16 s with 70 mA at 3.0 kV, and the replica was backed with carbon applied at an angle of 90°. The carbon-backed platinum replicas were lifted in clean water and transferred onto 400-mesh copper grids. Micrographs were recorded at a nominal magnification of 50,000× using a JEOL 1200EX-II transmission electron microscope at 80 kV (JEOL).

Measurement of Myosin Dimensions. Filament dimensions were determined with Metamorph software. The bare zone is the distance between the two closest heads at opposite ends of the bipolar minifilaments; the head area is the area within a line enclosing all the heads at one end of the bipolar minifilaments (Fig. 3).

ACKNOWLEDGMENTS. We thank Mathew Daniels for the use of the National Heart, Lung, and Blood Institute Electron Microscopy Core Facility. This research was supported by the Intramural Research Program of the National Heart, Lung, and Blood Institute, National Institutes of Health.

1. Liu X, et al. Regulation of actin-activated MgATPase of *Acanthamoeba* myosin II by phosphorylation of serine639 in loop 2. *Proc Natl Acad Sci USA*.
2. Maruta H, Korn ED (1977) *Acanthamoeba* myosin II. *J Biol Chem* 252(18):6501–6509.
3. Pollard TD, Stafford WF, Porter ME (1978) Characterization of a second myosin from *Acanthamoeba castellanii*. *J Biol Chem* 253(13):4798–4808.
4. Hammer JA, 3rd, Bowers B, Paterson BM, Korn ED (1987) Complete nucleotide sequence and deduced polypeptide sequence of a nonmuscle myosin heavy chain gene from *Acanthamoeba*: Evidence of a hinge in the rodlike tail. *J Cell Biol* 105(2):913–925.
5. Collins JH, Korn ED (1980) Actin activation of Ca^{2+}-sensitive Mg^{2+}-ATPase activity of *Acanthamoeba* myosin II is enhanced by dephosphorylation of its heavy chains. *J Biol Chem* 255(17):8011–8014.
6. Collins JH, Korn ED (1981) Purification and characterization of actin-activatable, Ca^{2+}-sensitive myosin II from *Acanthamoeba*. *J Biol Chem* 256(5):2586–2595.
7. Kuznicki J, Côté GP, Bowers B, Korn ED (1985) Filament formation and actin-activated ATPase activity are abolished by proteolytic removal of a small peptide from the tip of the tail of the heavy chain of *Acanthamoeba* myosin II. *J Biol Chem* 260(3):1967–1972.
8. Atkinson MAL, Appella E, Corigliano-Murphy MA, Korn ED (1988) Enzymatic activity and filament assembly of *Acanthamoeba* myosin II are regulated by adjacent domains at the end of the tail. *FEBS Lett* 234(2):435–438.
9. Atkinson MAL, Lambooy PK, Korn ED (1989) Cooperative dependence of the actin-activated Mg^{2+}-ATPase activity of *Acanthamoeba* myosin II on the extent of filament phosphorylation. *J Biol Chem* 264(7):4127–4132.
10. Ganguly C, et al. (1990) Regulation of the actin-activated ATPase activity of *Acanthamoeba* myosin II by copolymerization with phosphorylated and dephosphorylated peptides derived from the carboxyl-terminal end of the heavy chain. *J Biol Chem* 265(17):9993–9998.
11. Kuznicki J, Albanesi JP, Côté GP, Korn ED (1983) Supramolecular regulation of the actin-activated ATPase activity of filaments of *Acanthamoeba* Myosin II. *J Biol Chem* 258(10):6011–6014.
12. Pollard TD (1982) Structure and polymerization of *Acanthamoeba* myosin-II filaments. *J Cell Biol* 95(3):816–825.
13. Sinard JH, Pollard TD (1989) The effect of heavy chain phosphorylation and solution conditions on the assembly of *Acanthamoeba* myosin-II. *J Cell Biol* 109(4 Pt 1): 1529–1535.
14. Sinard JH, Stafford WF, Pollard TD (1989) The mechanism of assembly of *Acanthamoeba* myosin-II minifilaments: Minifilaments assemble by three successive dimerization steps. *J Cell Biol* 109(4 Pt 1):1537–1547.
15. Turbedsky K, Pollard TD (2005) Assembly of *Acanthamoeba* myosin-II minifilaments. Definition of C-terminal residues required to form coiled-coils, dimers, and octamers. *J Mol Biol* 345(2):351–361.
16. Sinard JH, Rimm DL, Pollard TD (1990) Identification of functional regions on the tail of *Acanthamoeba* myosin-II using recombinant fusion proteins. II. Assembly properties of tails with NH2- and COOH-terminal deletions. *J Cell Biol* 111(6 Pt 1):2417–2426.
17. Brzeska H, Korn ED (1996) Regulation of class I and class II myosins by heavy chain phosphorylation. *J Biol Chem* 271(29):16983–16986.
18. Pasternak C, Flicker PF, Ravid S, Spudich JA (1989) Intermolecular versus intramolecular interactions of Dictyostelium myosin: Possible regulation by heavy chain phosphorylation. *J Cell Biol* 109(1):203–210.
19. Liu X, et al. (1998) Filament structure as an essential factor for regulation of Dictyostelium myosin by regulatory light chain phosphorylation. *Proc Natl Acad Sci USA* 95(24): 14124–14129.
20. Ogihara S, Ikebe M, Takahashi K, Tonomura Y (1983) Requirement of phosphorylation of *Physarum* myosin heavy chain for thick filament formation, actin activation of Mg^{2+}-ATPase activity, and Ca^{2+}-inhibitory superprecipitation. *J Biochem* 93(1):205–223.
21. Sellers JR (1999) *Myosin* (Oxford Univ Press, Oxford, UK), 2nd Ed.
22. Murakami N, Healy-Louie G, Elzinga M (1990) Amino acid sequence around the serine phosphorylated by casein kinase II in brain myosin heavy chain. *J Biol Chem* 265(2): 1041–1047.
23. Murakami N, Singh SS, Chauhan VPS, Elzinga M (1995) Phospholipid binding, phosphorylation by protein kinase C, and filament assembly of the COOH terminal heavy chain fragments of nonmuscle myosin II isoforms MIIA and MIIB. *Biochemistry* 34(49):16046–16055.
24. Murakami N, Chauhan VPS, Elzinga M (1998) Two nonmuscle myosin II heavy chain isoforms expressed in rabbit brains: Filament forming properties, the effects of phosphorylation by protein kinase C and casein kinase II, and location of the phosphorylation sites. *Biochemistry* 37(7):1989–2003.
25. Dulyaninova NG, Malashkevich VN, Almo SC, Bresnick AR (2005) Regulation of myosin-IIA assembly and Mts1 binding by heavy chain phosphorylation. *Biochemistry* 44(18):6867–6876.
26. Ronen D, Ravid S (2009) Myosin II tailpiece determines its paracrystal structure, filament assembly properties, and cellular localization. *J Biol Chem* 284(37):24948–24957.
27. Hodge TP, Cross R, Kendrick-Jones J (1992) Role of the COOH-terminal nonhelical tailpiece in the assembly of a vertebrate nonmuscle myosin rod. *J Cell Biol* 118(5): 1085–1095.
28. Buxton DB, Adelstein RS (2000) Calcium-dependent threonine phosphorylation of nonmuscle myosin in stimulated RBL-2H3 mast cells. *J Biol Chem* 275(44):34772–34779.
29. Breckenridge MT, Dulyaninova NG, Egelhoff TT (2009) Multiple regulatory steps control mammalian nonmuscle myosin II assembly in live cells. *Mol Biol Cell* 20(1):338–347.
30. Dulyaninova NG, House RP, Betapudi V, Bresnick AR (2007) Myosin-IIA heavy-chain phosphorylation regulates the motility of MDA-MB-231 carcinoma cells. *Mol Biol Cell* 18(8):3144–3155.
31. Raab M, et al. (2012) Crawling from soft to stiff matrix polarizes the cytoskeleton and phosphoregulates myosin-II heavy chain. *J Cell Biol* 199(4):669–683.
32. Yonemura S, Pollard TD (1992) The localization of myosin I and myosin II in *Acanthamoeba* by fluorescence microscopy. *J Cell Sci* 102(Pt 3):629–642.
33. Kong H-H, Pollard TD (2002) Intracellular localization and dynamics of myosin-II and myosin-IC in live *Acanthamoeba* by transient transfection of EGFP fusion proteins. *J Cell Sci* 115(Pt 24):4993–5002.
34. Larochelle J, Gagnon A (1976) Osmoregulation in *Acanthamoeba castellanii*-II. Variations of the concentrations of some intracellular ions. *Comp Biochem Physiol* 54A:275–279.
35. Sinard JH, Pollard TD (1989) Microinjection into Acanthamoeba castellanii of monoclonal antibodies to myosin-II slows but does not stop cell locomotion. *Cell Motil Cytoskeleton* 12(1):42–52.